Frequency response of a viscoelastic tensegrity model: structural rearrangement contribution to cell dynamics

Patrick Cañadas, Sylvie Wendling-Mansuy, Daniel Isabey

Frequency Response of a Viscoelastic Tensegrity Model: Structural Rearrangement Contribution to Cell Dynamics

Patrick Cañadas[1]
CNRS UMR 5508 Laboratoire de Mécanique et Génie Civil (LMGC), Université Montpellier II, Montpellier, France

Sylvie Wendling-Mansuy
CNRS–USR 2164 Laboratoire d'Aérodynamique et Biomécanique du Mouvement, Université de la Méditerranée, Marseille, France

Daniel Isabey
INSERM, UMR 651, Fonctions Cellulaires et Moléculaires de l'Appareil Respiratoire et des Vaisseaux, Equipe Biomécanique Cellulaire et Respiratoire, Université Paris XII, Faculté de Médecine, Créteil, France

In an attempt to understand the role of structural rearrangement onto the cell response during imposed cyclic stresses, we simulated numerically the frequency-dependent behavior of a viscoelastic tensegrity structure (VTS model) made of 24 elastic cables and 6 rigid bars. The VTS computational model was based on the nonsmooth contact dynamics (NSCD) method in which the constitutive elements of the tensegrity structure are considered as a set of material points that mutually interact. Low amplitude oscillatory loading conditions were applied and the frequency response of the overall structure was studied in terms of frequency dependence of mechanical properties. The latter were normalized by the homogeneous properties of constitutive elements in order to capture the essential feature of spatial rearrangement. The results reveal a specific frequency-dependent contribution of elastic and viscous effects which is responsible for significant changes in the VTS model dynamical properties. The mechanism behind is related to the variable contribution of spatial rearrangement of VTS elements which is decreased from low to high frequency as dominant effects are transferred from mainly elastic to mainly viscous. More precisely, the elasticity modulus increases with frequency while the viscosity modulus decreases, each evolution corresponding to a specific power-law dependency. The satisfactorily agreement found between present numerical results and the literature data issued from in vitro cell experiments suggests that the frequency-dependent mechanism of spatial rearrangement presently described could play a significant and predictable role during oscillatory cell dynamics.

Keywords: cytoskeleton, cell rheology, time constant, structural viscosity, structural elasticity, oscillatory cell mechanics, frequency response

Introduction

Passive cell deformation resulting from the application of mechanical stress by neighboring cells or the microenvironment as well as stress-induced active cell response mediated by mechanotransduction are both fundamental processes involved in the control of many cellular functions such as differentiation, growth, DNA and/or protein synthesis, wound healing, and tissue remodeling [1–5]. The accomplishment of these cellular processes is possible because the cytoskeleton (CSK), i.e., a three-dimensional prestressed structure principally composed of a network of three types of interconnected filamentous biopolymers (actin filaments, microtubules, and intermediate filaments), spatially rearranges while CSK elements are redistributed throughout the multiscale CSK substructures which extend from the entire cell size (e.g., through stress fibers) down to an individual actin filament length [6–8]. Note that the "short-term" (or passive) stress/strain hardening of the CSK (let us say a minute or less) should not be confounded with the "long term" (or active) stress/strain hardening (let us say from hours to days or more). The latter is currently observed secondary to the active responses of the cell to imposed stimuli, e.g., CSK remodeling after sufficient exposure (i.e., hours) to fluid shear flow [9–11], activation of the acto-myosin contractile apparatus induced by several tens of minutes of cell compression using a microplates device [12]. The "short term" spatial rearrangement has already been thought to promote nonlinear effects such as stress-hardening behavior of the cell [13–17] or the internal tension dependence of cell rigidity [18–22]. Note that tension dependence of cell rigidity has recently been confirmed by Sultan et al. [23] who found a positive prestress dependence of the elastic modulus G' in both homogeneous and heterogeneous tensegrity structures close to the presently studied one. Noteworthy, recent experiments on micromanipulated living cells have revealed a more or less marked time (or frequency) dependence of the cellular mechanical response [12,24–28] with the expression of multiple time constants of cellular substructures (i.e., the number of cell-characteristic time constants would vary from two to infinite, depending on authors [24,29–32]).

Tensegrity models have been thought to be good candidates to describe the static behavior of cellular systems. There is at least two basic underlying assumptions for that: (i) tensegrity structures were proposed to model the CSK of stabilized adherent cells, i.e., these cells do not lose their mechanical integrity during the time of observation/measurement meaning that the rapid dynamic movement of peripheral actin filaments is not represented by such models; (ii) due to the spatial rearrangement of their elements, tensegrity structures can support large deformations still with no defect in their mechanical integrity [6,17–19,33–37]. Surprisingly, the frequency-dependent behavior of tensegrity structures has only been rarely studied while it could help to understand the contribution of rearrangement of structural elements to the cell response during imposed cyclic/oscillatory stresses. Sultan et al. [23] have used a slightly modified tensegrity structure made of viscoelastic elements in an attempt to fit experimental results. In fact, their model differs from the one presently studied both in terms of the number of constitutive elements (i.e., 36 structural

[1]Corresponding author.

elements in [23] and only 30 elements in the present study) and in terms of distribution of element viscoelastic properties (i.e., Sultan et al. have considered both a constant value of viscosity modulus and an arbitrary distribution of elastic modulus within the cables whereas we have used the same constant viscoelastic properties for all the cables in the present tensegrity structure). It appears from [23] that only a highly heterogeneous tensegrity model with a nonrealistic range of elastic properties could lead to quantitative agreement between experimental data and model prediction.

Thus, a number of key questions remain to be solved if one wants to better understand the contribution of the structural rearrangement in the oscillatory cell response. They concern (i) the variable contribution of spatial redistribution of elements as oscillatory frequency of the tensegrity structure changes, (ii) the relationships between the global properties of the structure, (i.e., time constants; elastic modulus; viscous modulus) and the local viscoelastic properties of constitutive elements, and (iii) the linearity assumption which is a point still under debate [38] which could not be considered in the Sultan et al. model while it is of prior interest in the oscillated tensegrity structure especially at large initial (or oscillatory) deformations [19]. Noteworthy, a frequency-dependent characterization of large-scale structural effects is required in the discussion about the exact nature of the cellular material. For instance, it would be of interest to estimate the contribution of spatial rearrangement of CSK elements on oscillatory cell mechanics.

In an attempt to answer the above questions, we used a recent computational model describing the mechanical behavior of a 30-element viscoelastic tensegrity structure (VTS model) anchored on the substrate through four attachment points previously used by our group to study the tensegrity response to transient stress loading [36,39]. To do so, we modified the loading conditions previously imposed transiently to the VTS model, to apply cyclic/oscillatory stresses. Mechanical properties of elements were maintained constant (i.e., a unique time constant characterizes all constitutive elements of the indeed homogeneous tensegrity structure) in order to capture the essential feature of the spatial redistribution effects and not the effect of an arbitrary heterogeneous distribution of individual properties as in [23]. Furthermore, we studied the influence of both the scale and the level of internal tension of the VTS model on the frequency response, which has not been studied in [23]. The tensegrity structure approach was justified because previous tensegrity model results were found at least in qualitative agreement with several experimental results. Although presently limited to low amplitude oscillations (i.e., less than 10% of oscillatory deformation of the VTS model) and no initial deformation (i.e., the VTS model is oscillated around its symmetrical resting shape), present results reveal that, depending on oscillatory frequency, behavior of the VTS model is modified because the weight of spatial redistribution of VTS elements varies as frequency changes. Such a mechanism is specifically revealed by oscillatory VTS model motion at fixed loading amplitudes.

Method

Constitutive Equations. The present viscoelastic tensegrity structure (VT structure) is composed of a discontinuous network of six bars compressed by a continuous network of 24 prestretched cables (Fig. 1). This model has been previously described and studied in steady-state conditions by simulating transient steps of loading (i.e., creep tests) [36,39]. At the reference state, where no external force is applied, the bars are aligned in pairs in the direction of the coordinate axes (Fig. 1). This symmetrical resting shape of the structure corresponds to the equilibrium between tension in cables and compression in bars [40,41]. In the present model, the bars are assumed to be rigid while each cable is assumed to behave like an elementary viscoelastic "Voigt" model (i.e., an "elastic" spring arranged in parallel with a "viscous" dashpot) supporting only tension. Cables may become to-

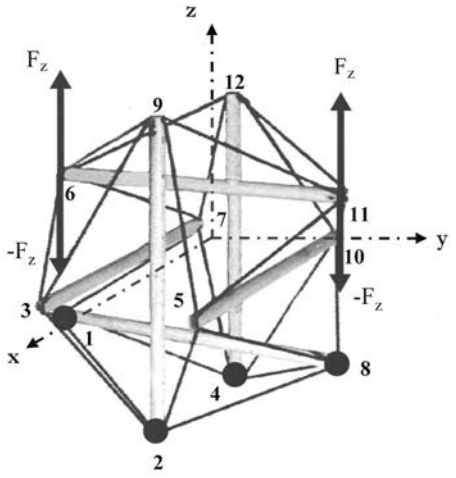

Fig. 1 Spatial view of the viscoelastic tensegrity structure (VTS) studied (6 bars and 24 viscoelastic cables). At the reference state (no external force applied to the structure), the four nodes {1, 2, 4, 8} are anchored and fixed in their spatial positions (●). The rectangular base {*x*, *y*, *z*} is the referential system. Oscillating forces (*Fz* and *–Fz*) are applied at nodal points {6, 11} along the *z* axis. The overall deformation of the VTS model is defined by the displacement along the *z* axis of the two nodes {6, 11} normalized by the bar length L_b which characterizes the size of the structure.

tally slacken if their actual length happens to be less than their natural resting length secondary to the interplay of compressive force on that cable.

The constitutive equations describe the dynamic behaviour of the VTS model taking into account the time dependence of cable properties and assuming linear viscoelasticity. They derive from the force equilibrium at each node and can be written by the following matrix equation of motion:

$$\{\mathrm{F}\} = [K(U)]\{U\} + [C(U)]\{\dot{\mathrm{U}}\} + [M(U)]\{\ddot{\mathrm{U}}\} \qquad (1)$$

where the external force vector {F} is related to (i) the nodal displacement vector {u} associated to the global rigidity matrix $[K(U)]$, (ii) the nodal displacement derivative or velocity vector $\{\dot{u}\}$ associated to the global damping matrix $[C(U)]$, and (iii) the nodal acceleration vector $\{\ddot{u}\}$ associated to the mass matrix $[M(U)]$. The force and nodal displacement/velocity/acceleration vectors are $[1 \times 36]$ column vectors and the rigidity/damping/mass matrices have a dimension $[36 \times 36]$ even before considering the boundary conditions (i.e., the external forces {F} applied and the four nodal linkages).

However, the numerical resolution of such a system of dynamic equations (Eq. (1)) appears difficult by using the common "finite element method" software (e.g., ABAQUS©) because the computation fails as soon as the tension in a given cable drops to zero secondary to the unilateral condition in the mechanical behaviour of cables [42]. In the aim to forestall this problem, we have developed a numerical model of the VTS model using a specific program (called LMGC90) based on the nonsmooth contact dynamics (NSCD) method ([43]; see also the Appendix). The latter has been originally developed to study short contact dynamic problems, such as divided medium mechanics.

In the NSCD method, the constitutive elements of the tensegrity structure are considered as a set of material points that mutually interact. The overall deformation of the tensegrity structure is deduced from the resolution of the following system of dynamic equations equivalent to Eq. (1) (see the Appendix):

$$[M(U)]\{\ddot{\mathrm{U}}\} = \{\mathrm{F}\} + \{\mathrm{r(U)}\} \tag{2}$$

where the column vector {r(U)} of the interactions between the material nodes satisfies unilateral conditions to the extent that cables remain stretched.

The interaction laws between two material nodes are defined by

$$\begin{cases} \bar{U} \geq 0 \\ R \geq 0 \\ \bar{U} \cdot R = 0 \end{cases} \quad \text{with} \quad \begin{cases} U = L - L_0 \\ \bar{U} = -U + \dfrac{1}{k} R \end{cases} \tag{3}$$

L (respectively, L_0) is the actual length (respectively, the resting length) of elements, i.e., cable or bar; k (=ES/L_0, with S its cross section) is the rigidity of the element, and R the reaction force between neighboring nodes. The unknowns of these conditions of complimentarily ($\bar{U}$;R) are taken into account in the problem (Eq. (2)) to resolve. Algorithms used for unilateral contact problems can directly resolve this problem, which is written at each increment of reequilibrium in the form of a system of linear equations with some constraints. The details of the resolution method of such problem are presented in [43] (see also the Appendix and [44]).

It should be noticed that the nodal mass is assumed to be weak (presently a few grams) and the VTS model is supposed to be not affected by gravity. These assumptions allow us a dynamical study of the VTS model by minimizing inertial effects, as inertial effects can mostly be neglected at micrometric sizes. Obviously, the rigidity and damping matrices of the general dynamic equation (Eq. (1)) are taken into account by the interaction vector {r(U)} of the equation rewritten by using the NSCD method (Eq. (2); see the Appendix and [42]).

Loading and Attachment Conditions of the VTS Model. External oscillatory forces are applied to the nodes 6 and 11 along the z axis (traction/compression cycles), while the "opposite" nodes (1, 2, 4, and 8) are assumed to be linked to a rigid nonplanar substratum via spherical joints (see Fig. 1). The applied oscillatory force (F) is then defined by

$$F(t) = F_0 \sin(2\pi f t) = F_0 \sin(\omega t) \tag{4}$$

where F_0 is the "constant" force magnitude and f (or ω) is the forced (angular) frequency.

Equation (Eq. (1)) appears to be a second-order differential equation with nonconstant second member. The general solution $U(t)$ is given by

$$\begin{aligned} U(t) = F_0 \Bigg\{ & \frac{1}{K} \Bigg(\frac{C - \sqrt{C^2 - 4KM}}{2\sqrt{C^2 - 4KM}} e^{-\frac{C+\sqrt{C^2-4KM}}{2M}t} \\ & \times \frac{C + \sqrt{C^2 - 4KM}}{2\sqrt{C^2 - 4KM}} e^{-\frac{C-\sqrt{C^2-4KM}}{2M}t} \Bigg) \cdots \\ & + \Bigg(\frac{K - \omega^2 M}{(K - \omega^2 M)^2 + \omega^2 c^2} \sin(\omega t) \\ & - \frac{\omega C}{(K - \omega^2 M)^2 + \omega^2 C^2} \cos(\omega t) \Bigg) \Bigg\} \end{aligned} \tag{5}$$

Hence, the global viscoelastic properties of the VTS model (i.e., elasticity E and viscosity η, moduli as well as time constant τ) were determined by curve fitting of the numerical data using (Eq. (5)), considering an equivalent global Voigt model, as done in previous studies [36,39].

Nondimensional Analysis. As in our previous studies on tensegrity structure [7,18,19,36,39,45], we normalized viscoelastic properties of the overall VTS model by their element properties, i.e.,

$$T^* = \frac{T_c^{(r)}}{(ES)_c} \quad (T_c^{(r)}\text{: elastic tension in each cable at reference state}) \tag{6}$$

$$L^* = \frac{L_b}{r_b} \quad (r_b\text{: bar radius}) \tag{7}$$

The normalized elastic tension T^* which corresponds to the elastic strain of cables at reference state, i.e., before loading, actually quantifies the basal level of internal tension in the VTS model and is actually equal to the initial strain of elastic elements. The normalized length L^* defines the characteristic scale of the overall 30-element tensegrity structure. Time constant (τ), structural elasticity modulus (E), and viscosity modulus (η) of the overall VTS model were normalized using cable properties, meaning that properties of the VTS model remain proportional to individual element properties:

$$\tau^* = \frac{\tau}{\tau_c} \tag{8}$$

$$E^* = \frac{E}{E_c} \tag{9}$$

$$\eta^* = \frac{\eta}{\eta_c} \tag{10}$$

Nodal displacement (U) of the loaded nodes (6 and 11) was normalized by taking into account the characteristic size of the structure (i.e., the bar length L_b) which defines an overall oscillatory deformation of the VTS model (ϵ_{osc}), whereas the applied frequency (f) was also normalized by taking into account cable time constant (τ_c)

$$\epsilon_{\mathrm{osc}} = \frac{U}{L_b} \tag{11}$$

$$f^* = f \times \tau_c \tag{12}$$

Results

The amplitude of oscillatory deformation (ϵ_{osc}) of the overall VTS model calculated at the level of oscillated nodes (Eq. (11)), as well as the structural viscoelastic properties of the global VTS model normalized by element properties (i.e., time constant τ^* (Eq. (8)), structural elasticity modulus E^* (Eq. (9)) and viscosity modulus η^* (Eq. (10)) are presented in Figs. 2–4 as a function of the normalized forced frequency f^* covering the range [10^{-4}–10^2]. Three zones of interest appear in these double logarithmic graphs (Figs. 2–4): (i) a low frequency zone ($f^* < 0.1$) with an oscillatory amplitude right below 10% ($\epsilon_{\mathrm{osc}} \sim 10\%$) where elastic effects predominate; (ii) an intermediate frequency zone ($0.1 \leq f^* \leq 10$) called transitional zone with a rapid change in the amplitude of oscillatory deformation ($0.1\% < \epsilon_{\mathrm{osc}} < 10\%$); where elastic and viscous effects are tightly balanced; and (iii) a high frequency zone ($f^* > 10$) with low amplitudes of oscillatory deformation ($\epsilon_{\mathrm{osc}} \sim 0.1\%$) where viscous effects predominate. Note that the elastic and viscous dominant zones appear symmetrically distributed on each side of a value of oscillatory frequency equal to the inverse of the cable time constant ($f \sim 1/\tau_c$, see Eq. (12)). Due to the decrease in oscillatory deformation amplitude (ϵ_{osc}) from low to high frequency, the contribution of spatial rearrangement of structural elements abruptly decreases as frequency increases (see Figs. 2–4). Noteworthy in the transitional zone, a satisfactorily curve fitting is given by the power law equation (i.e., $\epsilon_{\mathrm{osc}} \sim f^{*-0.83}$). By contrast, the two extreme elastic and viscous dominated zones are characterized by weak changes in ϵ_{osc} with frequency. The normalized time constant of the overall

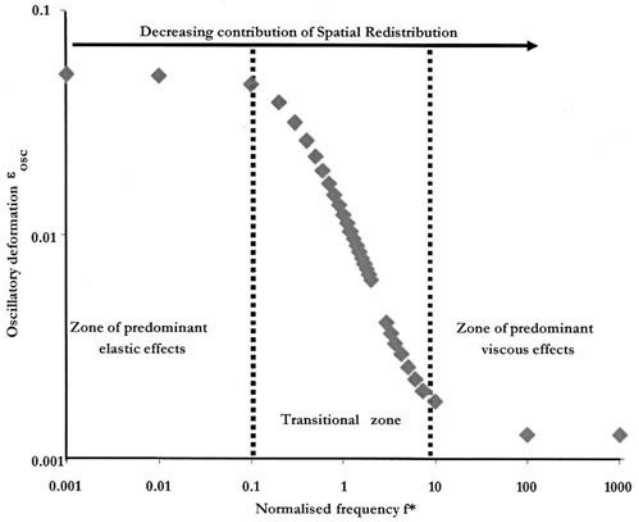

Fig. 2 Oscillatory deformation of the overall VTS as a function of the normalized forced frequency f^* in a double logarithmic scale. Three distinct zones could be distinguished: a low frequency zone ($f^*<0.1$) of roughly constant oscillatory deformation amplitude where elastic effects are predominant; a transitional zone ($0.1<f^*<10$) of a rapid change in the amplitude of the deformation (with a negative logarithmic slope (–0.83); and a satisfactory correlation coefficient $R^2=0.99$) where elastic and viscous effects are balanced and a high frequency zone ($f^*>10$) of low oscillatory deformation where viscous effects are predominant. The contribution of the spatial redistribution of the tensegrity structure appears to decrease when the frequency increases.

tensegrity model shown in Fig. 3, decreases nonlinearly with the oscillatory frequency within the transitional zone ($f^*=0.2-10$), following $\tau^* \sim f^{*-0.42}$. The frequency decrease in the overall time constant can be seen as a frequency-dependent solidifyinglike pro-

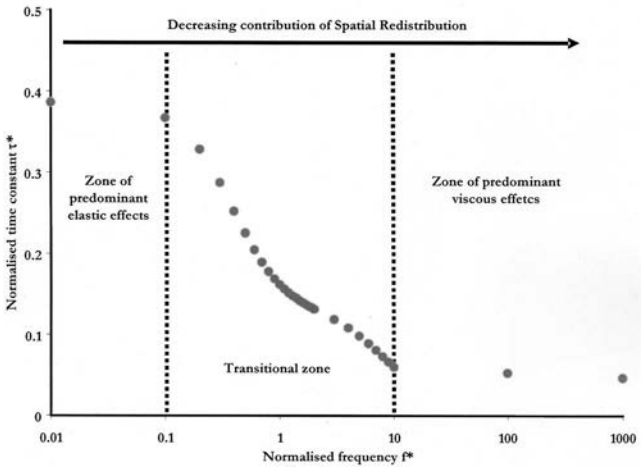

Fig. 3 Normalized time constant τ^* of the overall VTS model as a function of the normalized forced frequency f^* in a double logarithmic scale with the two zones of predominant (i) elastic ($f^*<1$) and (ii) viscous ($f^*>10$) effects, as well as the transitional zone ($0.1<f^*<10$). The normalized time constant of the overall tensegrity model decreases nonlinearly with the oscillatory frequency in the upper part of the transitional zone, following the power law $\tau^* \sim f^{*-0.42}$ with a correlation coefficient R^2(=0.97). The decreasing contribution of spatial redistribution of VTS elements contribute to the frequency-dependent solidifyinglike process for the VTS model.

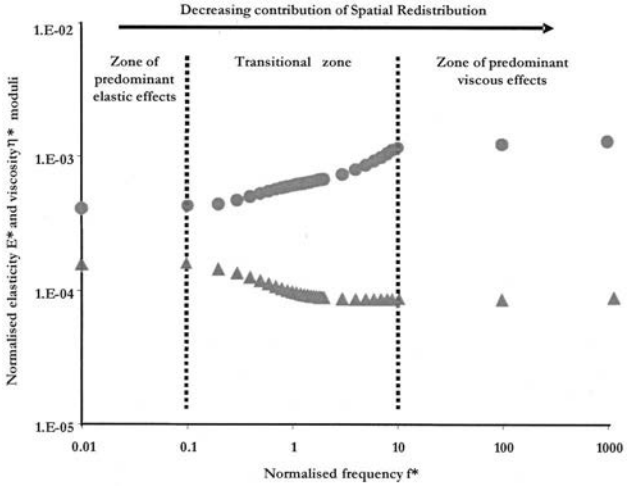

Fig. 4 Normalized viscosity modulus η^* and elasticity modulus E^* of the overall VTS model as a function of the normalized forced frequency f^* in a double logarithmic scale with the two zones of predominant elastic ($f^*<1$) and viscous ($f^*>10$) effects, and the transitional zone ($0.1<f^*<10$). The normalized elasticity modulus E^*(•) increases in the transitional zone with a logarithmic slope (+0.18) and the normalized viscosity modulus η^*(▲) decreases with a logarithmic slope (–0.24), the two with a correlation coefficient R^2(=0.99).

cess for the VTS model secondary to the decrease in the contribution of spatial redistribution of VTS elements. Interestingly, the normalized elasticity (E^*) and viscosity (η^*) moduli of the overall VTS model are, respectively, increased and decreased as oscillatory frequency increases. Noteworthy, frequency-dependent changes occur essentially within the transitional zone, exhibiting power laws which are, respectively, $E^* \sim f^{*+0.18}$ and $\eta^* \sim f^{*-0.24}$ in the frequency range ($f^*=0.2-10$) (see Fig. 4). It can be said that as frequency increases, the structure is dominated by two distinct mechanisms, i.e., a frequency-dependent hardeninglike process (E^* increases with f^*) and a frequency-dependent wateringlike process (η^* decreases with f^*) which both can be related to the decreasing contribution of spatial redistribution of VTS elements (ϵ_{osc} decreases as f^* increases as shown in Fig. 2).

Figures 5–9 present the variations of structural viscoelastic properties of the VTS model as a function of the normalized—and homogeneous—properties of its constitutive elements, i.e., length L^* and internal tension T^* (at reference state). Figure 5 shows the normalized time constant of the VTS model as a function of the normalized internal tension (T^*) obtained at the characteristic frequency $f^*=1$ and for a wide range of normalized elastic length L^* (=100, 1000, 10,000). Whatever the normalized length, the structural time constant decreases following a mean power law given by ($\tau^* \sim T^{*-0.42}$). Figures 6 and 7, respectively, show the variations of structural elasticity and viscosity moduli as a function of internal tension T^* still for $f^*=1$. The structural elasticity modulus E^* increases with the internal tension T^* following a power law close to $E^* \sim T^{*+0.52}$ for the three tested values of normalized length L^* (=100, 1000, 10,000). By contrast η^* which appears to be roughly constant in the low range of T^* values can be satisfactorily fitted by $\eta^* \sim T^{*+0.08}$ in the higher range (Fig. 7).

The results in Figs. 8 and 9 show that both normalized elasticity and viscosity moduli of the VTS model tested at $f^*=1$ are strictly proportional to the inverse of the square of the normalized length ($E^* \sim L^{*-2}$ and $\eta^* \sim L^{*-2}$). Accordingly, the structural time constant (τ^*) remains independent on the normalized element size L^* (data not shown). In other terms, when the size of a viscoelastic tensegrity structure is increased, its mechanical response to oscillatory loading is marked by a length-dependent softeninglike pro-

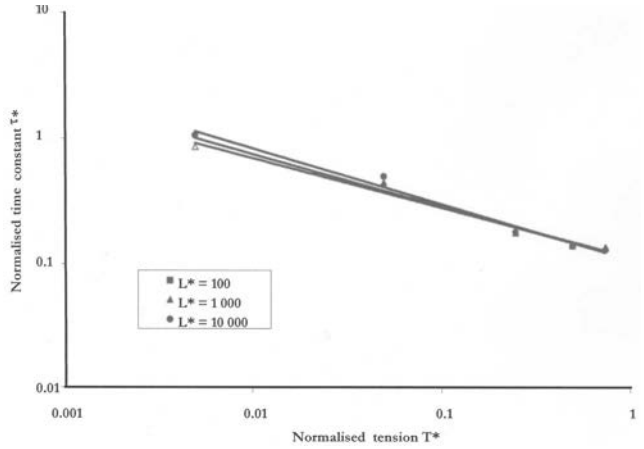

Fig. 5 Normalized time constant τ^* of the overall VTS as a function of the normalized internal tension (corresponding to the initial strain of the elastic cable) T^* for three different normalized element length L^* (=100, 1000, 10,000) in the transitional zone. τ^* decreases following a mean power law given by ($\tau^* \sim T^{*-0.42}$; $R^2=0.98$) whatever L^*. The values of τ^* decrease within a small range of [0.1-1] when T^* increases by two orders of magnitude, whatever the value of L^*.

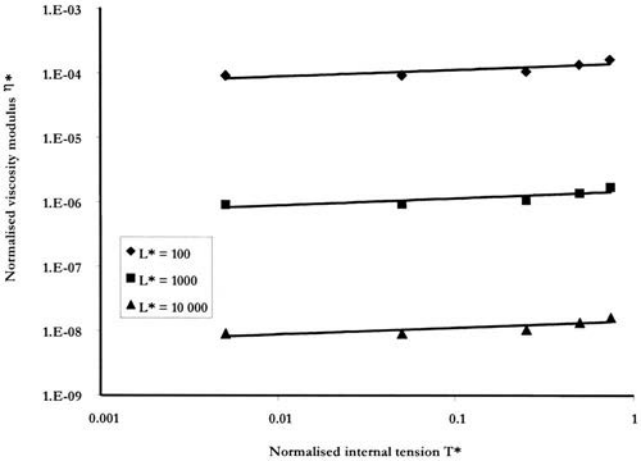

Fig. 7 Normalized viscosity modulus η^* of the overall tensegrity model as a function of the initial internal tension T^* for three different values of L^* (=100, 1000, 10,000) in the transitional zone. Viscosity modulus η^* is shown to increase nonsignificantly (logarithmic slope $\leq +0.1$; $R^2=0.98$) with increasing T^* for the three values of L^*.

cess (E^* decreases with L^*) and a length-dependent wateringlike process (η^* decreases with L^*), while the time response remains unaffected.

Discussion

The present study provides new data about the dynamical behavior of homogeneous viscoelastic tensegrity structure (VTS model) aiming to represent the contribution of structural rearrangement on the cytoskeleton behavior of adherent cells submitted to cycles of external oscillatory compression/extension. Consistently with previous studies, data are expressed in terms of nondimensional—universal—laws relating the fundamental parameters of the VTS model, i.e., dynamic properties of the whole VTS model (i.e., normalized time constant τ^*, normalized elasticity modulus E^*, normalized viscosity modulus η^*) versus (i) the imposed frequency normalized using the unique elastic element time constant, as well as (ii) the previously defined normalized physical properties of the VTS elements, i.e., internal tension T^* and elastic length L^* [18,19,36,39]. In a previous study performed on the same VTS model but during transient loading [36], we found that spatial rearrangement considered over a wide range of global strain ε_i (i.e., from zero up to 60%) was responsible for a variety of changes in structural dynamic properties, i.e., depending on the type of loading, τ^*; E^*; η^*, varied from a few percent to several hundred percent in the range $\epsilon_i = 0\% - 60\%$. In the present study performed in a lower range of amplitude of deformations ($\epsilon_{osc} < 10\%$, shown in Fig. 2), the frequency-dependent changes in elastic and viscous effects constitute a distinct frequency-dependent mechanism which is responsible for significant changes in VTS dynamic properties, i.e., $\tau^*(f^*)$; $E^*(f^*)$; $\eta^*(f^*)$, also vary significantly although within less than one order of magnitude (see Figs. 3 and 4). Noteworthy, this frequency-dependent mechanism, especially occurring in the range $f^* = 0.1 - 10$, is also associated to a variable contribution of the spatial redistribution of VTS elements as frequency changes (see Figs. 3 and 4) but it differs from the ϵ_i redistribution mechanism previously obtained (see Figs. 3–5 in [36]). Note that the presently found ϵ_{osc} redistri-

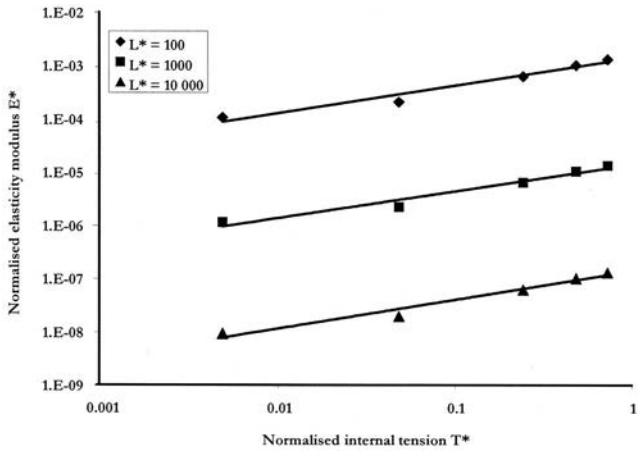

Fig. 6 Normalized elasticity modulus E^* of the overall viscoelastic tensegrity structure as a function of the normalized internal tension T^* for three different normalized element length L^* (=100, 1000, 10,000) in the transitional zone. E^* increases with T^* following a power law $E^* \sim T^{*0.52}$ ($R^2=0.97$) whatever the value of L^*. Note that the values of E^* decreases proportionally to the inverse of (L^{*2}) in the overall range of T^*.

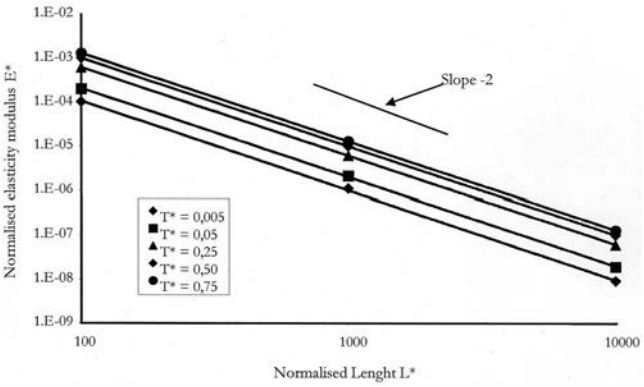

Fig. 8 Normalized elasticity modulus E^* as a function of the normalized length L^* for five different values of the internal tension T^* (= ♦ 0.005, ■ 0.05, ▲ 0.25, ♦ 0.5, • 0.75) in the transitional zone. Note that the curves show a strictly negative logarithmic slope (–2) whatever the value of T^*.

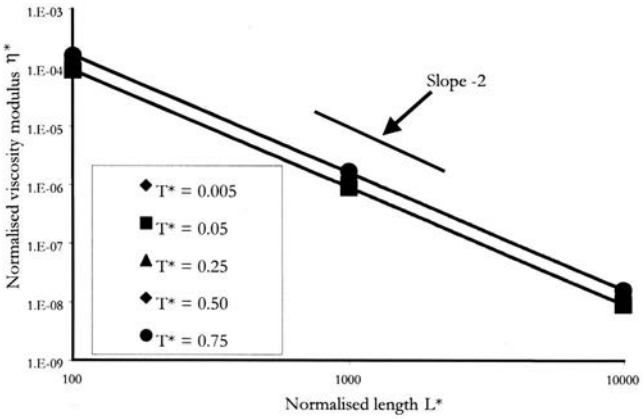

Fig. 9 Normalized viscosity modulus η^* as a function of the normalized length L^* for five different values of the internal tension T^* (= ♦ 0.005, ■0.05, ▲0.25, ♦ 0.5, •0.75) in the transitional zone. Note that the curves show a strictly negative logarithmic slope (–2) whatever the value of T^*.

bution mechanism (i) occurs even in the low amplitude range ($\epsilon_{osc} < 10\%$) and (ii) is maximized in a transitional zone of imposed frequency extending over one order of magnitude around the time constant of viscoelastic elements. In cases where the period of oscillatory loading ($=f^{-1}$) is significantly greater—at least one order of magnitude—than the characteristic time constant of VTS elastic elements ($f^* < 0.1$), the VTS model experiments maximum displacement amplitudes at a given force, i.e., the spatial redistribution of VTS elements is the highest (Fig. 2), whereas the speed at which viscoelastic elements change their length is sufficiently low that VTS elements reach close to their equilibrium state at each instant, thus going toward a quasistatic behavior (zone of predominant elastic effects in Figs. 2–4). In the opposite case ($f^* > 10$), i.e., the period of oscillatory loading ($=f^{-1}$) is significantly smaller than the characteristic time constant of VTS elements, the latter do not have enough time to experiment a large change in length (hence the small displacement amplitude of the VTS (Fig. 2)) and the energy is mostly spent to overcome friction instead of overcoming elastic recoil (zone of predominant viscous effects, Figs. 2–4). The intermediate frequency range ($0.1 \leq f^* \leq 10$) is a transitional zone where the respective weight of elastic and viscous effects rapidly changes with frequency. This transitional zone has been used to characterize the frequency-dependent changes of the structural properties. It should be noticed that the present approach allows us to focus on the role of spatial redistribution phenomena on ε_{osc} and mechanical properties of the structure, which is not possible from the Sultan et al.'s approach [23]. Moreover, present data were obtained on the basis of a full control of viscoelastic properties of the structural elements of the VTS model whereas in [23] the local elementary mechanical properties were found secondary to curve fitting of experimental data by using a different tensegrity model, that explain why present and Sultan et al. results are quite different. Furthermore, both the nodal attachment conditions and the loading applied differ between the two studies (i.e., three nodes fixed and an external force applied on the middle of a bar in [23]; four nodes fixed and two forces applied to the end of another bar in present study) and we have previously shown that similar tensegrity structures show different mechanical responses when attachment and loading conditions differ [36].

Following the same idea about frequency dependency of material mechanical properties, it is interesting to note that the frequencies applied in cell micromanipulation experiments (i.e., from 10^{-2} Hz to 1000 Hz; [29,30,46–49]) are embedded into the range of frequencies applied by Palmer et al. [50] on F-actin networks,

Table 1 Elasticity and viscosity moduli, hysteresivity and normalized forced frequency power law relationships obtained for the present theoretical VTS model, compared to those obtained in oscillatory cell experiments given in the literature [1–3]

	Numerical results on the VTS model	Living cell experiments (literature)
Elasticity modulus	$E^* \sim f^{0.18}$	G' proportional to f^x; $0.15 \leq x \leq 0.35$
Viscosity modulus	$\eta^* \sim f^{-0.24}$	(G''/ω) proportional to f^y; $-1 < y < 0$
Hysteresivity	$h \sim f^{0.58}$	Constant up to $f \sim 10$ Hz Increase from $f \sim 10$ Hz

with great similarities in the results obtained: Up to a value of applied frequency ~10 Hz, both the living cells and the F-actin networks exhibit a roughly constant ratio in between the dissipative modulus (G'') associated to the viscosity and the storage modulus (G') associated to the elasticity of the tested materials. In other terms, that means that both the living cells and the F-actin networks reveal corresponding time constants, i.e., from fractions of seconds to several seconds (see below).

Confirming previous results obtained in transient loading conditions on the same VTS model [36], results obtained during oscillatory loading conditions reveal that L^* (Figs. 8 and 9) and to a lesser extent T^* (Figs. 6 and 7), have a more marked effect—than f*—on the structural viscoelastic properties. Due to the L^{*-2} dependence of oscillatory elasticity (E^*) and viscous (η^*) moduli, it appears that an increase in L^* by a decade would result in a decrease in E^* and η^* by two decades, meaning that L^* is a quite sensitive parameter. By contrast, almost two decades of an increase in T^* are necessary to expect a single decade of increase in E^* or of decrease in τ^*, meaning that the oscillatory viscous modulus η^* is only very slightly dependent on T^*. Because these results are expressed in terms of L^* and T^* dependencies of elastic and viscosity moduli and time constant, they can be compared to previous results obtained by our group (i) on a similar VTS model submitted to a step of force and responding by a creep function [36] and (ii) on a geometrically similar but purely elastic tensegrity structure submitted to constant forces [19], corresponding to zero frequency. This means that power laws found to describe the T^* and L^* dependencies in the purely elastic structure should approach that found at the lowest frequency value tested in the present study (i.e., $f^* = 0.001$).

We present below a table of viscoelastic properties exhibiting the different power law relationships obtained in the present theoretical VTS study and compare it with experimental results obtained in oscillatory cell experiments (see Table 1). Note that oscillatory cell experiments were mainly performed in a low range of cell deformation amplitudes (i.e., practically below 500 nm). Noteworthy, the power-laws established from oscillatory response of the VTS model, in addition to reinforce previous VTS results obtained with transient loading [36,39], fall in the range of frequency dependence founded in living cell experiments [30,46–49,51]. Such a consistency between VTS theory and oscillatory cell mechanics suggests that the reported frequency-dependent effects could actually be associated to the variable weight of the spatial rearrangement of CSK filaments following a mechanism similar to the low amplitude mechanism described above. Another important similarity between the VTS models and cellular experiments concerns the common assumption that inertia of nodes, or of CSK elements, is negligible due to the micrometric size of biological objects. This is why fundamental equations of the oscillatory VTS motion only consider the rigidity and the damping matrices.

Present results suggest that the frequency-dependent mechanism of structural reorganization presently described in the low

amplitude range of VTS oscillatory deformations might contribute to explain the frequency-dependent cell behavior found in living cell experiments. First, experiments performed on a variety of adherent cells (e.g., smooth muscle cells; alveolar epithelial cells A549; bronchiolar epithelial cells BEAS-2B, and C2 myoblasts) which are submitted to oscillatory loadings imposed by a variety of micromanipulation methods (e.g., magnetic twisting cytometry (MTC) [29,30,49], atomic force microscopy (AFM) [46,47], laser tracking microrheology (LTM) [32], and optical tweezers (OT) [48] could be reanalyzed on light with the present results. Maksym et al. [30] and Fabry et al. [29] have investigated the frequency response of the cytoskeleton in smooth muscle cells using the classical MTC technique or the optical MTC technique within very different ranges of imposed frequencies (e.g., [0.05–0.4 Hz] for Maksym et al. and [0.01–1000 Hz] for Fabry et al. These authors have found similar power laws between (i) the elasticity modulus (G') and the frequency, i.e., $G' \sim f^{0.20}$, (ii) the viscosity modulus (defined as the ratio $G''/(2\pi f)$), and the frequency (f), i.e., $G''/(2\pi f)^{-1} \sim \mathrm{f}^{-1}$ in Maksym et al. [30] and, respectively, $G' \sim f^{0.17}$ and $G''/(2\pi f) \sim f^{x}$ with the power coefficient x increasing from values above -1 up to below zero as frequency increases (see Table 1). Noteworthy, these experimental relationships do not disagree with the results established by Puig-de-Morales et al. [49] who have used a similar MTC technique to investigate mechanical properties of bronchial epithelial cell (BEAS-2B), i.e., $G' \sim f^{0.25}$ and $G''/(2\pi f) \sim f^{-0.75}$ in the frequency range (0.03–16 Hz). Furthermore, Alcaraz et al. [47] have found similar relationships by applying atomic force microscopy to the study of A549 and BEAS-2B, within the frequency range (0.1–100 Hz), i.e., $G' \sim f^{0.22}$ for A549 cell lines (respectively, $G' \sim f^{0.20}$ for BEAS-2B) and $G''/(2\pi f) \sim f^{x}$ (with $x=-0.8$ at frequency <10 Hz). Moreover, as f increases, the power coefficient x decreased toward 0 but never reached this value, which is similar to the study by Fabry et al. These results do not contradict those of Yamada et al. [32] which have used the laser tracking microrheology method (range of frequency: (0.016–4775 Hz) to establish that for kidney epithelial cells, the complex modulus $G^*: |G^*| \sim f^{0.75}$, that corresponds also to the results obtained by Palmer et al. [50] on F-actin networks (see above). Recent measurements performed with optical tweezers by Balland et al. [48] in C2 myoblasts show power-laws $G' \sim f^{a}$ with $0.15 \leq a \leq 0.35$ and $G''/(2\pi f) \sim f^{b}$ with $-0.65 \leq b \leq -0.85$, in the frequency range [0.01–50 Hz]. Noteworthy, the present power-law established in terms of frequency dependence of the structural elasticity properties from the VTS model (i.e., $E^* \sim f^{0.18}$) fits remarkably with cell experimental results (i.e., which vary from $G' \sim f^{0.15}$ to $G' \sim f^{0.35}$), meaning that the frequency-dependent stress-hardening behavior experimentally observed on adherent cells could advantageously be explained and predicted by spatial rearrangement predicted by tensegrity model. Furthermore, the frequency-watering behavior (i.e., decrease in viscosity modulus) found in these experimental studies might also be described and predicted by a similar mechanism, with however some difference logically explainable by the contribution of complementary mechanisms such as heterogeneity in time constants distributed throughout the CSK structure or possibly, viscous effects induced by cytosolic fluid movements whose contribution might be reinforced in the high frequency zone. Indeed, in all experiments performed in living cells as well as in actin solutions, the low frequency global behavior mostly reflects the structure while, at high frequency, the global behavior seems to be influenced by a viscous fluid contribution (see for example [29] or also [50]). However, such a fluid contribution at high frequencies is beyond the present topic since the VTS model never departs from a pure solid by definition. Hence, presently found power law relationships might appear insufficient to cover the differences founded in living cells between low and high frequencies. Nevertheless, due to the unique time constant used to define the constitutive cables, the present results are particularly pertinent to describe the structural behavior in the transitional zone in which the ϵ_{osc}-redistribution mechanism is maximized. Note that the transitional zone is centered on a peculiar frequency which happens to be the inverse value of the unique time constant of all cables. Noteworthy, at such a frequency, elastic and viscous behavior were nearly balanced. Note also that in the transitional zone, normalized frequency f^* varies from 0.1 to 10 which corresponds to time constants varying by two orders of magnitude. Thus, proposed normalized power laws in the transitional region describe the variable contribution of the structure in a region taking into account that time constants of elements could be different and vary within a wide range.

In addition, Maksym et al. [30] have observed that depolymerizing F-actin with cytochalasin D (a drug whose effect has been thought to decrease internal tension [18]) produced (i) a decrease in CSK elasticity modulus and (ii) no significant alteration of the CSK viscosity modulus (that also means that the time constant increases when the CSK-tension decreases), that can be related to the T^* dependency of E^*, η^*, and τ^* established for the VTS model. In particular, the proposed relationships could provide quantitative predictions of the effect of low concentrations of cytochalasin D which result in a decrease CSK-internal tension [18]. Indeed, Maksym et al. [30] have shown that adding 1 mg/ml of cytochalasin D—after 16 min ± 1.8 min of exposure—results in a mean diminution by about 40% of cell elasticity modulus (see Fig. 10 in [30]). The present VTS model in which the found T^* dependence of E^* is $E^* \sim T^{*+0.52}$ predicts a diminution by 40% of normalized elasticity E^* for a decrease in T^* by about 65% (initial strain). In other terms, present results obtained on the VTS model suggest that adding 1 mg/ml of cytochalasin D to medium of living cells would produce (after 16 min of exposure) a diminution by 65% of CSK internal tension.

Furthermore, it appears from experimental studies that, whatever the cell type and more generally whatever the characteristic size of the CSK substructure considered, living cells exhibit a common feature expressed by the nondimensional ratio between the stored and the dissipated energies. This feature is described by a constant value of a nondimensional parameter ($h = G''/G' = \tau \times \omega$) called hysteresivity, which expresses the interdependence between stored elastic energy and viscous losses [29,30,47,49,52]. We find in the present study that the VTS model exhibits a non-negligible frequency dependence of VST hysteresivity, i.e., $h \sim f^{0.58}$ ($R^2 = 0.99$, data not shown), which contrasts with experimental observations in which h is roughly constant for living cells ($h \approx 0.3$–0.4). In fact, to exhibit a constant hysteresivity h ($= \tau \times \omega$), a structure or a material should definitely exhibit a time constant corresponding to each frequency tested, i.e., practically a quasi infinite number of time constants. This is obviously not the case of the homogeneous VTS model presently studied. However, it should be underlined that present data demonstrate that spatial rearrangement mechanism, herein quantified in an homogeneous VTS, tends to enhance the number of characteristic time constants since the VTS time constant is different, actually decreased, from the time constant of identical VTS elements (see Fig. 3). Extending this result to the CSK requires to consider that not one, but a number of CSK substructures have to be taken into account. In a previous study [24], we found that living adherent epithelial cells exhibit, at first glance, at least two time constants corresponding to a cortical and a deep CSK components with, respectively, a fast and a slow response. Moreover, there are some reasons to believe that each CSK component behaves as a tensegrity structure with its own characteristic length, internal tension, and number of elements, e.g., short, slightly tensed but numerous cortical elements compared to long, highly tensed and numerously limited deep elements [7]. All these parameters would have a specific effect on the normalized elasticity modulus meaning that, depending on the integrated level at which a CSK substructure is considered, it should exhibit a specific time constant. Other micromanipulation studies suggest that an infinite number of time constants is re-

quired to describe the complexity of the multiscale interconnected CSK network [29,51]. Therefore, it is easy to imagine that oscillating a CSK structure at a unique frequency results in a wide variety of normalized frequencies through the variety of time constant characterizing each CSK substructure, each normalized frequency corresponding to a specific attenuation of the local time constant through the mechanism of spatial redistribution actually predictable by the present theory. Further studies on an improved VTS model, constituted by several realistic time constants could bring supplementary arguments on the frequency dependency of the living cell mechanical responses, at the light of the structural rearrangement of CSK.

Acknowledgment

We are indebted to Professor M. Jean (Laboratoire de Mécanique et d'Acoustique, CNRS UPR 7051, Marseille, France) and Dr. F. Dubois (Laboratoire de Mécanique et de Génie Civil, CNRS UMR 5508, Montpellier, France) for their contributions.

Appendix

In divided medium mechanics, if it is considered two bodies O and O' as following:

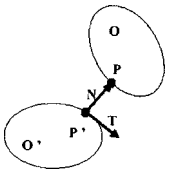

One may define the so-called *candidate to contact* (or simply *contact*) the unique couple constituted by a candidate object O associated to its contactor P and an antagonist object O' associated to its contactor P'. It can be then defined by the vector PP' a unitary normal vector N and a unitary tangent vector T. It can be also defined (i) the components of the relative speed of P related to O': $U(U_N, U_T)$, (ii) the components of the reaction force exerted by O' to O: $R(R_N, R_T)$, and (iii) the gap g as the distance between P and P'. In such a case, the *Signorini Conditions* can be written as follow [43]:

$$g \geq 0 \quad R_N \geq 0 \quad g \cdot R_N = 0 \tag{A1}$$

This condition can also be written in speed terms [53] for an initial time $t_0, g(t_0) \geq 0$, whatever the time range ($t \in I$), the function $U_N(t)$ is defined by

$$\text{if } g(t) \leq 0 \quad \text{then} \quad U_N(t) \geq 0 \quad R_N(t) \geq 0 \quad U_N(t) \cdot R_N(t) = 0 \tag{A2}$$

The above conditions (A1) and (A2) can be represented in the following *Signorini graph*:

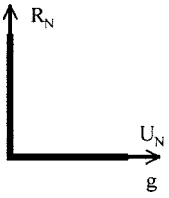

In the case of a cable constituting a tensegrity structure, i.e., a cable that can only be stretched by applying traction forces while it is totally slacken if a compression force is applied, we can define the free length l_0 and the actual length l when a traction force is applied. So, the relationships relating the tension (T) to both the length (l) and the rigidity (k) of the cable are

$$\begin{aligned} &\text{if } -(l - l_0) \geq 0 \quad \text{then} \quad -T = -k(l - l_0) \\ &\text{if } -(l - l_0) \geq 0 \quad \text{then} \quad T = 0 \end{aligned} \tag{A3}$$

The corresponding *Signorini graph is*

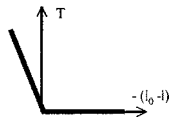

Thus, if one wants to replace Eqs. (A3) in a classic Signorini scheme, one can write

$$\bar{R} = T - k(l - l_0) \quad \text{and} \quad \bar{U} = -(l - l_0) \tag{A4}$$

As a result, the Signorini condition and the associated graphic become

$$\bar{R} \geq 0 \quad \bar{U} \geq 0 \quad \bar{U} \,.\, \bar{R} = 0 \tag{A5}$$

and

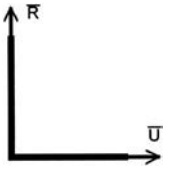

This method has been already applied to the study of several tensegrity structures, differing in terms of number of elements and we have yet verify the applicability of such en original approach to the study of the mechanical properties of tensegrity models [44].

References

[1] Pavalko, F. M., Chen, N. X., Turner, C. H., Burr, D. B., Atkinson, S., Hsieh, Y. F., Qiu, J., and Duncan, R. L., 1998, "Fluid Shear-Induced Mechanical Signaling in MC3T3-E1 Osteoblasts Requires Cytoskeleton-Integrin Interactions," Am. J. Physiol., **275**, pp. C1591–C1601.

[2] Planus, E., Galiacy, S., Matthay, M., Laurent, V., Gavrilovic, J., Murphy, G., Clérici, C., Isabey, D., Lafuma, C., and d'Ortho, M. P., 1999, "Role of Collagenase in Mediating In Vitro Alveolar Epithelial Wound Repair," J. Opt. Soc. Am. B, **112**(2), pp. 243–252.

[3] Bereiter-Hahn, J., 1994, "Functional Morphology and Biomechanics," Verh. Dtsch. Zool. Ges., **87**(2), pp. 129–145.

[4] Elson, E. L., 1988, "Cellular Mechanism as an Indicator of CSK Structure and Function," Annu. Rev. Biophys. Biophys. Chem., **17**, pp. 397–430.

[5] Vico, L., Lafage-Proust, M. H., and Alexandre, C., 1998, "Effects of Gravitational Changes on the Bone System In Vitro and In Vivo," Bone (N.Y.), **22**(5), pp. 95S–100S.

[6] Ingber, D. E., 2000, "Opposing Views on Tensegrity as a Structural Framework for Understanding Cell Mechanics," J. Appl. Physiol. **89**(4), pp. 1663–1670.

[7] Laurent, V. M., Cañadas, P., Fodil, R., Planus, E., Asnacios, A., Wendling, S., and Isabey, D., 2002, "Tensegrity Behaviour of Cortical and Cytosolic Cytoskeletal Components in Twisted Living Adherent Cells," Acta Biotheor., **50**(4), pp. 331–356.

[8] Forgacs, G., 1995, "On the Possible Role of Cytoskeletal Filamentous Networks in Intracellular Signaling: An Approach Based on Percolation," J. Cell. Sci., **108**(6), pp. 2131–2143.

[9] Choquet, D., Felsenfeld, D. P., and Sheetz, M. P., 1997, "Extracellular Matrix Rigidity Causes Strengthening of Integrin-Cytoskeleton Linkages," Cell, **88**(1), pp. 39–48.

[10] Davies, P. F., 1995, "Flow-Mediated Endothelial Mechanotransduction," Physiol. Rev., **75**(3), pp. 519–560.

[11] Davies, P. F., Barbee, K. A., Volin, M. V., Robotewskyj, A., Chen, J., Joseph, L., Griem, M. L., Wernick, M. N., Jacobs, E., Polacek, D. C., DePaola, N., and Barakat, A. L., 1997, "Spatial Relationships in Early Signaling Events of Flow-Mediated Endothelial Mechanotransduction," Annu. Rev. Physiol., **59**, pp. 527–549.

[12] Thoumine, O., and Ott, A., 1997, "Time Scale Dependent Viscoelastic and Contractile Regimes in Fibroblasts Probed by Microplate Manipulation," J. Cell. Sci., **110**, pp. 2109–2116.

[13] Dennerll, T. J., Buxbaum, R. E., and Heidemann, S. R., 1988, "Tension and Compression in the Cytoskeleton of PC-12 Neurites II: Quantitative Measurements," J. Cell Biol., **107**(2), pp. 665–664.

[14] Heidemann, S. R., and Buxbaum, R. E., 1990, "Tension as a Regulator and Integrator of Axonal Growth," Cell Motil. Cytoskeleton, **17**, pp. 6–10.

[15] Heidemann, S. R., Kaech, S., Buxbaum, R. E., and Matus, A., 1999, "Direct Observations of the Mechanical Behaviors of the Cytoskeleton in Living Fibroblasts," J. Cell Biol., **145**(1), pp. 109–122.

[16] Maniotis, A. J., Chen, C. S., and Ingber, D. E., 1997, "Demonstration of Mechanical Connections between Integrins, Cytoskeletal Filaments and

Nucleoplasm that Stabilize Nuclear Structure," Proc. Natl. Acad. Sci. U.S.A., **94**, pp. 849–854.
[17] Wang, N., Butler, J., and Ingber, D., 1993, "Mechanotransduction Across the Cell Surface and Through the Cytoskeleton," Science, **260**, pp. 1124–1127.
[18] Wendling, S., Planus, E., Laurent, V. M., Barbe, L., Mary, A., Oddou, C., and Isabey, D., 2000, "Role of Cellular Tone and Microenvironmental Conditions on Cytoskeleton Stiffness Assessed by Tensegrity Model," Eur. Phys. J.: Appl. Phys., **9**, pp. 51–62.
[19] Wendling, S., Oddou, C., and Isabey, D., 1999, "Stiffening Response of a Cellular Tensegrity Model," J. Theor. Biol., **196**(3), pp. 309–325.
[20] Wang, N., Tolic-Norrelykke, I. M., Chen, J., Mijailovich, S. M., Butler, J. P., Fredberg, J. J., and Stamenovic, D., 2002, "Cell Prestress I. Stiffness and Prestress are closely associated in Adherent Contractile Cells," Am. J. Physiol.: Cell Physiol., **282**, pp. 606–616.
[21] Stamenovic, D., Liang, Z., Chen, J., and Wang, N., 2002a, "Effect of the Cytoskeletal Prestress on the Mechanical Impedance of Cultured Airway Smooth Muscle Cells," J. Appl. Physiol., **92**(4), pp. 1443–1450.
[22] Stamenovic, D., Mijailovich, S. M., Tolic-Norrelykke, I. M., Chen, J., and Wang, N., 2002b, "Cell Prestress II. Contribution of Microtubules," Am. J. Physiol.: Cell Physiol., **282**, pp. 617–624.
[23] Sultan, C., Stamenovic, D., and Ingber, D. E., 2004, "A Computational Tensegrity Model Predicts Dynamic Rheological Behaviors in Living Cells," Ann. Biomed. Eng., **32**(4), pp. 520–530.
[24] Laurent, V. M., Fodil, R., Canadas, P., Fereol, S., Louis, B., Planus, E., and Isabey, D., 2003, "Partitioning of Cortical and Deep Cytoskeleton Responses From Transient Magnetic Bead Twisting," Ann. Biomed. Eng., **31**(10), pp. 1263–1278.
[25] Baush, A. R., Moller, W., and Sackman, E., 1999, "Measurements of Local Viscoelasticity and Forces in Living Cells by Magnetic Tweezers," Biophys. J., **76**, pp. 573–579.
[26] Mathur, A. B., Truskey, G. A., and Reichert, W. M., 2000, "Atomic Force and Total Reflection Fluorescence Microscopy for the Study of Force Transmission in Endothelial Cells," Biophys. J., **78**, pp. 1725–1735.
[27] Satcher, R. L., and Dewey, C. F., 1996, "Theoretical Estimates of Mechanical Properties of the Endothelial Cell Cytoskeleton," Biophys. J., **71**, pp. 109–118.
[28] Thoumine, O., and Ott, A., 1997, "Comparison of the Mechanical Properties of Normal and Transformed Fibroblasts," Biorheology, **34**(4/5), pp. 309–326.
[29] Fabry, B., Maksym, G. N., Butler, J. P., Glogauer, M., Navajas, D., and Fredberg, J. J., 2001, "Scaling the Microrheology of Living Cells," Phys. Rev. Lett., **87**(14), pp. 148102–148105.
[30] Maksym, G. N., Fabry, B., Butler, J. P., Navajas, D., Tschumperlin, D. J., Laporte, J. D., and Fredberg, J. J., 2000, "Mechanical Properties of Cultured Human Airway Smooth Muscle Cells From 0.05 to 0.4 Hz," J. Appl. Physiol., **89**, pp. 1619–1632.
[31] Wu, H. W., Kuhn, T., and Moy, V. T., 1998, "Mechanical Properties of L929 Cells Measured by Atomic Force Microscopy: Effects of Anticytoskeletal Drugs and Membrane Crosslinking," Scanning, **20**, pp. 389–397.
[32] Yamada, S., Wirtz, D., and Kuo, S. C., 2000, "Mechanics of Living Cells Measured by Laser Tracking Microrheology," Biophys. J., **78**, pp. 1736–1747.
[33] Stamenovic, D., Ingber, D. E., Wang, N., and Fredberg, J. J., 1996, "A Microstructural Approach to Cytoskeletal Mechanics Based on Tensegrity," J. Theor. Biol., **181**, pp. 125–136.
[34] Stamenovic, D., and Coughlin, M. F., 1999, "The Role of Prestress and Architecture of the Cytoskeleton and Deformability of Cytoskeletal Filaments in Mechanics of Adherent Cells: A Quantitative Analysis," J. Theor. Biol., **201**, pp. 63–74.
[35] Volokh, K. Y., Vilnay, O., and Belsky, M., 2000, "Tensegrity Architecture Explains Linear Stiffening and Predicts Softening of Living Cells," J. Biomech., **33**, pp. 1543–1549.
[36] Cañadas, P., Laurent, V. M., Oddou, C., Isabey, D., and Wendling, S., 2002, "A Cellular Tensegrity Model to Analyse the Structural Viscoelasticity of the Cytoskeleton," J. Theor. Biol., **218**, pp. 155–173.
[37] Ingber, D., 2003, "Tensegrity I. Cell Structure and Hierarchical Systems Biology," J. Cell. Sci., **116**, pp. 1157–1173.
[38] Ohayon, J., Tracqui, P., Fodil, R., Féréol, S., Laurent, V. M., Planus, E., and Isabey, D., 2004, "Analysis of Nonlinear Responses of Adherent Epithelial Cells Probed by Magnetic Bead Twisting: A Finite Element Model Based on An Homogenization Approach," J. Biomech. Eng., **126**(6), pp. 685–698.
[39] Cañadas, P., Laurent, V. M., Chabrand, P., Isabey, D., and Wendling-Mansuy, S., 2003, "Mechanisms Governing the Visco-Elastic Responses of Living Cells Assessed by Foam and Tensegrity Models," Med. Biol. Eng. Comput., **41**(6), pp. 733–739.
[40] Mohri, F., and Motro, R., 1993, "Static and Kinematic Determination of Generalized Space Reticulated Systems," Struct. Eng. Rev., **5**(3), pp. 231–237.
[41] Pugh, A., 1976, *Introduction to Tensegrity*, University of California Press, Berkeley and Los Angeles, CA.
[42] Wendling, S., Cañadas, P., Oddou, C., and Meunier, A., 2002, "Interrelations Between Elastic Energy and Strain in a Tensegrity Model; Contribution to the Analysis on the Mechanical Response in Living Cells," Comput. Methods Biomech. Biomed. Eng., **5**(1), pp. 1–6.
[43] Jean, M., 1999, "The Non-Smooth Contact Dynamics Method," Appl. Mech. Eng., **177**, pp. 235–257.
[44] Wendling, S., Cañadas, P., and Chabrand, P., 2003, "Toward a Generalized Tensegrity Model Describing the Mechanical Behaviour of the Cytoskeleton Structure," Comput. Methods Biomech. Biomed. Eng., **1**, pp. 1–8.
[45] Wendling, S., Oddou, C., and Isabey, D., 2000, "Approche Structurale de la Mécanique du Cytosquelette: Solide Alvéolaire vs Modèle de Tenségrité," C. R. Acad. Sci., Ser. IIb Mec. Phys. Astron., **328**, pp. 97–104.
[46] Rubin, C., Turner, A. S., Mallinckrodt, C., Jerome, C., Mcleod, K., and Bain, S., 2002, "Mechanical Strain Induced Noninvasively in the High-Frequency Domain, is Anabolic," Bone (N.Y.), **30**(3), pp. 445–452.
[47] Alcaraz, J., Buscemi, L., Grabulosa, M., Trepat, X., Fabry, B., Farre, R., and Navajas, D., 2003, "Microrheology of Human Lung Epithelial Cells Measured by Atomic Force Microscopy," Biophys. J., **84**, pp. 2071–2079.
[48] Balland, M., Richert, A., and Gallet, F., 2005, "The Dissipative Contribution of Myosin II in the Cytoskeleton Dynamics of Myoblasts," Eur. Biophys. J., **34**(3), pp. 255–261.
[49] Puig-de-Morales, M., Millet, E. J., Fabry, B., Navajas, D., Wang, N., Butler, J. P., and Fredberg, J. J., 2004, "Cytoskeletal Mechanics in Adherent Human Airway Smooth Muscle Cells: Probe Specificity and Scaling of Protein-Protein Dynamics," Am. J. Physiol.: Cell Physiol. **287**, pp. 643–654.
[50] Palmer, A., Mason, T. G., Xu, J., Kuo, S. C., and Wirtz, D., 1999, "Diffusing Wave Spectroscopy Microrheology of Actin Filament Networks," Biophys. J., **76**, pp. 1063–1071.
[51] Fabry, B., Maksym, G. N., Butler, J. P., Glogauer, M., Navajas, D., Taback, N. A., Millet, E. J., and Fredberg, J. J., 2003, "Time Scale and Other Invariants of Integrative Mechanical Behavior in Living Cells," Phys. Rev. E, **68**(4), 041914, pp. 1–18.
[52] Fredberg, J. J., and Stamenovic, D., 1989, "On the Imperfect Elasticity of Lung Tissue," J. Appl. Physiol., **67**(6), pp. 2408–2419.
[53] Cambou, B., and Jean, M., 2001, *Micromécanique des Matériaux Granulaires*, Hermes Science Publication, Paris, France.